AGU PUBLICATIONS

Geophysical Research Letters

RESEARCH LETTER
10.1002/2014GL060334

Key Points:
- Surprisingly different behavior of Na and K in the upper mesosphere is explained
- Development of a new K chemistry model within a 3-D chemistry-climate model

Supporting Information:
- Readme
- Table S1 and Figures S1–S3

Correspondence to:
J. M. C. Plane,
j.m.c.plane@leeds.ac.uk

Citation:
Plane, J. M. C., W. Feng, E. Dawkins, M. P. Chipperfield, J. Höffner, D. Janches, and D. R. Marsh (2014), Resolving the strange behavior of extraterrestrial potassium in the upper atmosphere, *Geophys. Res. Lett.*, *41*, 4753–4760, doi:10.1002/2014GL060334.

Received 25 APR 2014
Accepted 13 JUN 2014
Accepted article online 18 JUN 2014
Published online 3 JUL 2014

The copyright line for this article was changed on 7 August 2014 after original online publication.

Resolving the strange behavior of extraterrestrial potassium in the upper atmosphere

J. M. C. Plane[1], W. Feng[1,2], E. Dawkins[2], M. P. Chipperfield[2], J. Höffner[3], D. Janches[4], and D. R. Marsh[5]

[1]School of Chemistry, University of Leeds, Leeds, UK, [2]School of Earth and Environment, University of Leeds, Leeds, UK, [3]Leibniz Institute of Atmospheric Physics, Kühlungsborn, Germany, [4]Space Weather Laboratory, NASA Goddard Space Flight Center, Greenbelt, Maryland, USA, [5]National Center for Atmospheric Research, Boulder, Colorado, USA

Abstract It has been known since the 1960s that the layers of Na and K atoms, which occur between 80 and 105 km in the Earth's atmosphere as a result of meteoric ablation, exhibit completely different seasonal behavior. In the extratropics Na varies annually, with a pronounced wintertime maximum and summertime minimum. However, K varies semiannually with a small summertime maximum and minima at the equinoxes. This contrasting behavior has never been satisfactorily explained. Here we use a combination of electronic structure and chemical kinetic rate theory to determine two key differences in the chemistries of K and Na. First, the neutralization of K^+ ions is only favored at low temperatures during summer. Second, cycling between K and its major neutral reservoir $KHCO_3$ is essentially temperature independent. A whole atmosphere model incorporating this new chemistry, together with a meteor input function, now correctly predicts the seasonal behavior of the K layer.

1. Introduction

The ablation of meteoroids in the upper atmosphere leads to the formation of distinct layers of metal atoms around 90 km. These layers, which are global in extent, provide a sensitive marker for the dynamics and chemistry of the atmosphere at the edge of space [*Plane*, 2003]. The presence of K atoms in the mesosphere and lower thermosphere (MLT) was first established from photometric observation of the twilight emission at 766.5 and 769.9 nm [*Sullivan and Hunten*, 1964]. Subsequent work using the resonance lidar technique [*Megie et al.*, 1978; *Eska et al.*, 1999] showed that the K column density varies semiannually, with maxima in summer and winter and minima at the equinoxes. The layer thus exhibits little overall seasonal variation at midlatitudes. In contrast, the Na layer has a pronounced annual variation, being around 3 times larger in winter than summer [*Marsh et al.*, 2013]. As a result, the Na/K abundance ratio at midlatitudes decreases from ~50 in winter to only ~10 during summer. The explanation for this very surprising difference in behavior between two Group 1 (alkali) metals, whose chemistry should be very similar, is a problem of 50 years' standing.

Initially, attention focused on whether the Na/K ratio indicated a seasonal change in the source of the metals in the MLT. The Na/K elemental ratio in meteoroids is around 15, whereas the seawater ratio is 47, suggesting that the vertical transport of sea-salt particles during storms in the polar night could be responsible for the wintertime enhancement of Na over K, which is greatest at high latitudes [*Sullivan and Hunten*, 1964; *Megie et al.*, 1978]. However, in addition to the challenge of transporting material upward within the winter polar vortex to the MLT where the mean wind is downward, *Jegou et al.* [1980] showed that the mesospheric Na/Li ratio remains constant or may even decrease during winter, which appears to rule out a sea-salt source. An alternative explanation proposed that the neutral metal atom chemistry in the MLT is controlled by the dynamics of hydrated metal ion clusters [*Jegou et al.*, 1985], but the assumed temperature-dependent differences in the ion cluster chemistries required for this model have not subsequently been validated by experiment or theory. More recent modeling attempts [*Eska et al.*, 1999; *Delgado et al.*, 2006] have been unable to identify key differences in the chemistry of K and Na.

K^+ ions have been observed by rocket-borne mass spectrometry in a permanent layer above 90 km [*Kopp*, 1997]. These ions form continuously from K in the MLT via photoionization and charge transfer with ambient ions [*Eska et al.*, 1999]:

$$K + h\nu \rightarrow K^+ + e^- \quad (1)$$

$$K + NO^+ \rightarrow K^+ + NO \quad (2)$$

$$K + O_2^+ \rightarrow K^+ + O_2 \quad (3)$$

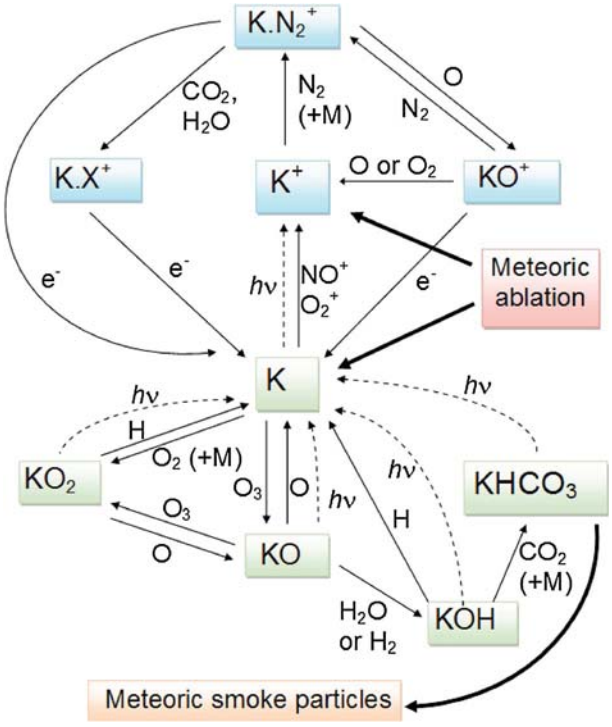

Figure 1. Schematic diagram of the important reaction pathways for K and K^+ produced by meteoric ablation in the MLT. Neutral and ionic K species are enclosed in green and blue boxes, respectively. Thin black lines depict chemical reactions; broken lines indicate photochemical processes. In this scheme, the main neutral reservoir is $KHCO_3$, which is permanently removed as a constituent of meteoric smoke.

Neutralization of K^+ occurs by forming a cluster ion with a ligand X, where $X = N_2$, O_2, O (in order of decreasing concentration in the MLT). These clusters can then undergo ligand switching with another atmospheric component Y (CO_2 or H_2O) to form a more stable cluster, before undergoing dissociative electron recombination:

$$K^+ + X(+M) \rightleftharpoons K^+ \cdot X \quad (4)$$

$$K^+ \cdot X + Y \rightarrow K^+ \cdot Y + X \quad (5)$$

$$K^+ \cdot (X \text{ or } Y) + e^- \rightarrow K + X \text{ or } Y \quad (6)$$

where M is a third body (most likely N_2 or O_2). *Plane et al.* [2006] carried out high-level quantum chemistry calculations on the $K^+ \cdot X$ and $\cdot X \cdot K^+ \cdot Y$ cluster ions and then used Rice-Ramsperger-Kassel-Markus (RRKM) theory to estimate the rate coefficients for reactions (4) and (5). The important result is that because K^+ is a relatively large singly charged ion (cf. Na^+), it forms very weakly bound clusters with the major species (N_2, O_2, and O) in the MLT, with binding energies less than 20 kJ mol^{-1}. The sequence of reactions (4)–(6) therefore only becomes significant at the very low temperatures characteristic of the summertime MLT. Figure 1 illustrates schematically the important pathways that couple K^+ and K in the MLT.

Although the ion-molecule chemistry described above should produce an enhancement of K during summer, *neutral* chemistry would be expected, by analogy with Na [*Plane*, 2004], to remove K through formation of stable reservoir species. In the case of Na, the important reservoir is sodium bicarbonate ($NaHCO_3$), which is only converted back to atomic Na by photolysis or reaction with H. The reaction $NaHCO_3 + H \rightarrow Na + H_2CO_3$ has an activation energy of about 10 kJ mol^{-1} [*Cox et al.*, 2001]. Thus, during summer the reaction becomes very slow, causing $NaHCO_3$ to build up and contributing to the observed minimum in the Na column density [*Plane*, 2004].

In this paper we use a combination of theoretical techniques to explore the analogous chemistry of potassium. The resulting rate coefficients for the neutral reactions, together with those from our previous study of K ion-molecule reactions [*Plane et al.*, 2006], are then incorporated into a whole atmosphere chemistry-climate model.

2. Theoretical Calculations on Neutral K Chemistry

In order to calculate rate coefficients and photolysis rates, a variety of electronic structure calculations was performed using the Gaussian 09 suite of programs [*Frisch et al.*, 2009]. Initially, the hybrid density functional/Hartree-Fock B3LYP method was employed with the 6-311 + G(2d,p) triple zeta basis set, which has both polarization and diffuse functions added to the atoms. Excited state calculations were performed using the time-dependent TD/B3LYP method [*Bauernschmitt and Ahlrichs*, 1996]. Very accurate energies of the stationary points (i.e., local minima and transition states) on the relevant potential energy surfaces (PESs) were calculated at the complete basis set (CBS-QB3) level of theory [*Montgomery et al.*, 1999]. In the case of the KO radical, the CBS-QB3 method failed due to excessive mixing of the frozen core and valence orbitals in the coupled cluster step of the calculation. Accurate reaction enthalpies for reactions involving KO were therefore carried out at the B3LYP level using the augmented version of the relativistic small-core effective core potential ECP10MDF basis set of the Stuttgart/Cologne group [*Lim et al.*, 2005].

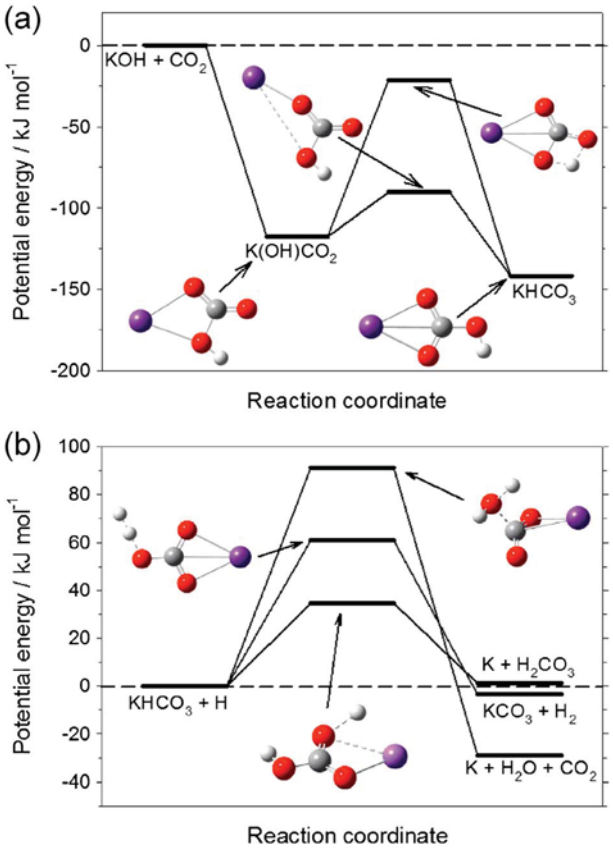

Figure 2. (a) Potential energy surface for the recombination of KOH and CO_2 to form the reservoir species $KHCO_3$. (b) Potential energy surface for the reaction between $KHCO_3$ and H, illustrating the three lowest-energy reaction channels. Color scheme: K (purple), O (red), H (white), and C (grey).

As shown in Figure 1, K atoms are oxidized by O_3 to yield KO, which a second O_3 can then oxidize to KO_2 [*Plane*, 2002]. KO_2 also forms directly from the recombination of K and O_2 [*Plane et al.*, 1990]. However, in the MLT these oxides exist in the presence of O, H, H_2, H_2O, and CO_2. Calculations (see above) show that the following reactions are all exothermic:

$$\mathrm{KO + O \rightarrow K + O_2} \quad \Delta H(0\ \mathrm{K}) = -243\ \mathrm{kJ\ mol^{-1}} \tag{7}$$

$$\mathrm{KO + H_2O \rightarrow KOH + OH} \quad \Delta H(0\ \mathrm{K}) = -1\ \mathrm{kJ\ mol^{-1}} \tag{8}$$

$$\mathrm{KO + H_2 \rightarrow KOH + H} \quad \Delta H(0\ \mathrm{K}) = -57\ \mathrm{kJ\ mol^{-1}} \tag{9}$$

$$\mathrm{KO_2 + O \rightarrow KO + O_2} \quad \Delta H(0\ \mathrm{K}) = -138\ \mathrm{kJ\ mol^{-1}} \tag{10}$$

$$\mathrm{KO_2 + H \rightarrow K + HO_2} \quad \Delta H(0\ \mathrm{K}) = -85\ \mathrm{kJ\ mol^{-1}} \tag{11}$$

$$\mathrm{KOH + H \rightarrow K + H_2O} \quad \Delta H(0\ \mathrm{K}) = -171\ \mathrm{kJ\ mol^{-1}} \tag{12}$$

Reaction (9) has a second channel forming $K + H_2O$ which is exothermic by 228 kJ mol^{-1}. However, in the case of the analogous $NaO + H_2$ reaction, formation of Na is the minor channel [*Ager and Howard*, 1987] and we assume the same for K. Reaction (11) could also form KOH + O, which is exothermic by 135 kJ mol^{-1} but involves breaking the strong O—O bond in the superoxide and is therefore probably slow.

The potential energy surfaces of reactions (7)–(12) do not contain significant energy barriers, and so by analogy with the corresponding reactions of NaO and NaO_2 [*Ager and Howard*, 1987; *Helmer and Plane*, 1993; *Griffin et al.*, 2001], these reactions are likely to be fast with little temperature dependence. We therefore assign them a typical collision theory rate coefficient of 2×10^{-10} exp(−120/*T*) cm^3 $molecule^{-1}$ s^{-1}.

KOH can also recombine with CO_2 to form the bicarbonate:

$$\mathrm{KOH + CO_2 (+ M) \rightarrow KHCO_3} \quad \Delta H(0\ \mathrm{K}) = -142\ \mathrm{kJ\ mol^{-1}} \tag{13}$$

Figure 2a illustrates the potential curve for reaction (13), together with the geometries of the stationary points (atom coordinates are listed in Table S1 in the supporting information). The KOH and CO_2 initially recombine to form the $K(OH)CO_2$ adduct. This adduct then rearranges to the more stable $KHCO_3$ either via migration of the H or the K atom, the latter having a much lower energy barrier with respect to the energy of the reactants. The rate coefficient for reaction (13) was calculated using a multiwell energy-grained master equation solved with the program Master Equation Solver for Multienergy Well Reactions [*Robertson et al.*, 2008], where the microcanonical rate coefficients linking the reactants, intermediates, and products were calculated by RRKM theory using the molecular parameters in Table S1 (supporting information). The internal energies of the intermediates on the PES were divided into a contiguous set of grains (width 100 cm^{-1}), each containing a bundle of rovibrational states. For dissociation to products or reactants, microcanonical rate coefficients were determined using inverse Laplace transformation to link them directly to the dipole-induced dipole capture rate coefficient [*Georgievskii and Klippenstein*, 2005], $k_{\mathrm{capture}}(\mathrm{KOH + CO_2}) = 5.8 \times 10^{-10}\ (T/300\ \mathrm{K})^{1/6}$ cm^3 $molecule^{-1}$ s^{-1}. The probability of collisional transfer between grains was estimated using the exponential down model (average energy for downward transitions

was set to $< \Delta E >_{down} = 300\ cm^{-1}$, assumed temperature independent). At the low-pressure limit appropriate for the MLT region, $k_{13}(140–220\ K) = 7.1 \times 10^{-28}\ (200\ K/T)^{4.21}\ cm^6\ molecule^{-2}\ s^{-1}$.

$KHCO_3$ could potentially be destroyed by reaction with H or O:

$$KHCO_3 + H \rightarrow K + H_2CO_3 \qquad \Delta H(0\ K) = 1\ kJ\ mol^{-1} \tag{14a}$$

$$\rightarrow KCO_3 + H_2 \qquad \Delta H(0\ K) = -3\ kJ\ mol^{-1} \tag{14b}$$

$$\rightarrow K + H_2O + CO_2 \qquad \Delta H(0\ K) = -29\ kJ\ mol^{-1} \tag{14c}$$

$$KHCO_3 + O \rightarrow KCO_3 + OH \qquad \Delta H(0\ K) = 8\ kJ\ mol^{-1} \tag{15}$$

These reactions are either exothermic or only slightly endothermic and so were investigated in more detail. Figure 2b shows the potential energy curves and transition state geometries for the three channels of reactions (14a)–(14c). Channels (14a)–(14c) have barriers of 32, 61, and 71 kJ mol^{-1}, respectively. Channels (14b) and (14c) can therefore be ruled out at MLT temperatures. The rate coefficient for reaction (14a) was estimated to be $k_{14a}(140–220\ K) = 4.5 \times 10^{-11}\ \exp(-3590/T)\ cm^3\ molecule^{-1}\ s^{-1}$ by using transition state theory with a correction for tunneling of H through the reaction barrier, assumed to be a symmetrical Eckart barrier as in our previous study of the analogous reaction of $NaHCO_3$ [*Cox et al.*, 2001] (see Table S1 in the supporting information for the relevant molecular parameters). At the various levels of theory used in this study, the energy barrier for $KHCO_3 + H$ is consistently between 7.1 and 9.3 kJ mol^{-1} higher than that for $NaHCO_3 + H$. Thus, even allowing for some uncertainty in the calculated *absolute* value of the barrier for reaction (14a), the reaction should be at least 2 orders of magnitude slower at 200 K than its Na analogue. Reaction (15) has a significant barrier of 38 kJ mol^{-1} and will therefore be too slow in the MLT for further consideration.

The photolysis cross sections for $KHCO_3$, KO_2, and KOH as a function of wavelength were calculated at the TD/B3LYP/6-311 + g(2d,p) level of theory [*Frisch et al.*, 2009] and then placed on an absolute scale using our previously measured cross sections for the Na analogues [*Self and Plane*, 2002]. The photolysis rates of these three potential molecular reservoirs were estimated to be 1.2×10^{-4}, 2.2×10^{-3}, and $0.027\ s^{-1}$, respectively. Figure S1 (supporting information) illustrates the cross-section spectra for $KHCO_3$ and $NaHCO_3$, which have thresholds around 280 nm.

Finally, the dimerization rate coefficient of $KHCO_3$ was estimated from the dipole-dipole capture rate [*Georgievskii and Klippenstein*, 2005] to be $1.0 \times 10^{-9}\ (T/200\ K)^{-0.29}\ cm^3\ molecule^{-1}\ s^{-1}$, using a calculated value for the dipole moment of $KHCO_3$ of 8.2 Debye (at the B3LYP/6-311 + g(2d,p) level). However, $KHCO_3$ can also polymerize with other meteoric constituent molecules (e.g., $NaHCO_3$, FeOH, and $Mg(OH)_2$), and the dimerization rate coefficient needs to be increased to account for this. The meteoritic elemental ratios of Na, Fe, Mg, and Si relative to K are 15.5, 248, 279, and 264, respectively [*Asplund et al.*, 2009]. Thus, the concentration of compounds containing these other elements could potentially be ~800 times higher than the concentration of $KHCO_3$. However, recent modeling studies [*Vondrak et al.*, 2008; *Feng et al.*, 2013; *Langowski et al.*, 2014] indicate that Fe, Mg, and Si ablate with much lower efficiencies than K (and Na), so the polymerization rate coefficient should be estimated by increasing the dimerization rate coefficient by significantly less than 800. A factor of 270 (i.e., a phenomenological polymerization rate coefficient of $2.7 \times 10^{-7}\ cm^3\ molecule^{-1}\ s^{-1}$) was found to reproduce the observed underside of the K layer satisfactorily, as shown below.

3. Atmospheric Modeling

Table 1 contains a complete list of rate coefficients for the neutral and ion-molecule reactions depicted in Figure 1. In order to model the K layer, we adopt the same approach that was used recently to model the global Na, Fe, and Mg layers [*Feng et al.*, 2013; *Marsh et al.*, 2013; *Langowski et al.*, 2014]. Three components are combined to construct the K model (termed here WACCM-K): (i) the Whole Atmosphere Climate Community Model (WACCM, version 4), a "high-top" coupled chemistry-climate model with an upper boundary at 6.0×10^{-6} hPa (~140 km); (ii) a description of the neutral and ion-molecule chemistry of K (Figure 1 and Table 1); and (iii) the meteoroid input function (MIF), which specifies the temporal and geographical input of meteoric metallic atoms into the MLT [*Marsh et al.*, 2013].

Table 1. Neutral and Ionic Gas-Phase Reactions in the Potassium Model

Number[a]	Reaction	Rate Coefficient[b]	Source
	Neutral Chemistry		
R1	$K + O_3 \rightarrow KO + O_2$	$1.15\times10^{-9}\ \exp(-120/T)$	1
R2 (7)	$KO + O \rightarrow K + O_2$	$2\times10^{-10}\ \exp(-120/T)$	2
R3	$K + O_2\ (+M) \rightarrow KO_2$	$1.3\times10^{-29}\ (T/200)^{-1.23}$	3
R4	$KO + O_3 \rightarrow KO_2 + O_2$	$6.9\times10^{-10}\ (\exp(-385/T)$	1
R6 (10)	$KO_2 + O \rightarrow KO + O_2$	$2\times10^{-10}\ \exp(-120/T)$	2
R7 (8)	$KO + H_2O \rightarrow KOH + OH$	$2\times10^{-10}\ \exp(-120/T)$	2
R8 (9)	$KO + H_2 \rightarrow KOH + H$	$2\times10^{-10}\ \exp(-120/T)$	2
R9 (11)	$KO_2 + H \rightarrow K + HO_2$	$2\times10^{-10}\ \exp(-120/T)$	2
R10 (12)	$KOH + H \rightarrow K + H_2O$	$2\times10^{-10}\ \exp(-120/T)$	2
R11 (13)	$KOH + CO_2\ (+M) \rightarrow KHCO_3$	$7.1\times10^{-28}\ (T/200)^{-4.2}$	4
R12 (14a, 14b, 14c)	$KHCO_3 + H \rightarrow K + H_2CO_3$	$4.5\times10^{-11}\ \exp(-3590/T)$	5
R13	$KHCO_3 + KHCO_3\ (+M) \rightarrow$ dimer	$270\times[1\times10^{-9}\ (T/200)^{-0.29}]$	6
	Ion-molecule Chemistry		
R20 (2)	$K + NO^+ \rightarrow K^+ + NO$	9.4×10^{-10}	7
R21 (3)	$K + O_2^+ \rightarrow K^+ + O_2$	3.2×10^{-9}	7
R22 (4)	$K^+ + N_2\ (+M) \rightarrow K^+\cdot N_2$	$2.3\times10^{-30}\ (T/200)^{-2.39}$	7
R-22	$K^+\cdot N_2\ (+M) \rightarrow K^+ + N_2$	$2.8\times10^{-8}\ \exp(-1680/T)$	7
R23 (4)	$K^+ + O_2\ (+M) \rightarrow K^+\cdot O_2$	$1.2\times10^{-30}\ (T/200)^{-2.12}$	7
R-23	$K^+\cdot O_2^+\ (+M) \rightarrow K^+ + O_2$	$1.5\times10^{-9}\ \exp(-820/T)$	7
R24 (4)	$K^+ + O\ (+M) \rightarrow K^+\cdot O^+$	$8.8\times10^{-32}\ (T/200\ \mathrm{K})^{-1.28}$	7
R-24	$K^+\cdot O^+\ (+M) \rightarrow K^+ + O$	$2.6\times10^{-10}\ \exp(-1800/T)$	7
R25 (4)	$K^+ + CO_2\ (+M) \rightarrow K^+\cdot CO_2$	$1.3\times10^{-29}\ (T/200)^{-2.43}$	7
R26 (4)	$K^+ + H_2O\ (+M) \rightarrow K^+\cdot H_2O$	$3.0\times10^{-29}\ (T/200)^{-2.22}$	7
R27 (5)	$K^+\cdot N_2 + O \rightarrow K^+\cdot O + N_2$	$2.9\times10^{-10}\ (T/200\ \mathrm{K})^{-0.17}$	7
R-27 (5)	$K^+\cdot O + N_2 \rightarrow K^+\cdot N_2 + O$	$2.5\times10^{-11}\ (T/200\ \mathrm{K})^{-0.55}$	7
R28 (5)	$K^+\cdot N_2 + CO_2 \rightarrow K^+\cdot CO_2 + N_2$	$4.8\times10^{-10}\ (T/200\ \mathrm{K})^{-0.88}$	7
R-28 (5)	$K^+\cdot CO_2 + N_2 \rightarrow K^+\cdot N_2 + CO_2$	$2.8\times10^{-10}\ \exp(-2220/T)$	7
R29 (5)	$K^+\cdot O_2 + O \rightarrow K^+\cdot O + O_2$	$2.8\times10^{-10}\ (T/200\ \mathrm{K})^{-0.42}$	7
R-29 (5)	$K^+\cdot O + O_2 \rightarrow K^+\cdot O_2 + O$	$5.0\times10^{-10}\ \exp(-752/T)$	7
R30 (5)	$K^+\cdot O + CO_2 \rightarrow K^+\cdot CO_2 + O$	$7.1\times10^{-10}\ (T/200\ \mathrm{K})^{-0.21}$	7
R-30 (5)	$K^+\cdot CO_2 + O \rightarrow K^+\cdot O + CO_2$	$1.4\times10^{-9}\ \exp(-2200/T)$	7
R31 (5)	$K^+\cdot O + H_2O \rightarrow K^+\cdot H_2O + O$	$7.1\times10^{-10}\ (T/200\ \mathrm{K})^{-1.90}$	7
R32 (5)	$K^+\cdot O_2 + N_2 \rightarrow K^+\cdot N_2 + O_2$	$1.6\times10^{-10}\ (T/200\ \mathrm{K})^{-0.90}$	7
R-32 (5)	$K^+\cdot N_2 + O_2 \rightarrow K^+\cdot O_2 + N_2$	$1.0\times10^{-9}\ \exp\ (-873/T)$	7
R33 (5)	$K^+\cdot O_2 + CO_2 \rightarrow K^+\cdot CO_2 + O_2$	$1.5\times10^{-10}\ (T/200\ \mathrm{K})^{-1.94}$	7
R34 (5)	$K^+\cdot O_2 + H_2O \rightarrow K^+\cdot H_2O + O_2$	$1.8\times10^{-9}\ (T/200\ \mathrm{K})^{-0.99}$	7
R35 (5)	$K^+\cdot N_2 + H_2O \rightarrow K^+\cdot H_2O + N_2$	$2.4\times10^{-9}\ (T/200\ \mathrm{K})^{-0.45}$	7
R36 (5)	$K^+\cdot CO_2 + H_2O \rightarrow K^+\cdot H_2O + CO_2$	$1.4\times10^{-9}\ (T/200\ \mathrm{K})^{-1.26}$	7
R37 (6)	$KX^+ + e^- \rightarrow K + X$ ($X = O, O_2, N_2, CO_2, H_2O$)	$1\times10^{-6}\ (T/200)^{-1/2}$	8
	Photochemical Reactions		
R38	$KO_2 + h\nu \rightarrow K + O_2$	2.2×10^{-3}	9
R39	$KOH + h\nu \rightarrow K + OH$	2.7×10^{-2}	9
R40	$KHCO_3 + h\nu \rightarrow K + HCO_3$	1.2×10^{-4}	9
R41 (1)	$K + h\nu \rightarrow K^+ + e^-$	4×10^{-5}	10

[a]The number in parenthesis refers to the number used when the reaction is listed in the text.
[b]Rate coefficient units: unimolecular, s^{-1}; bimolecular, $cm^3\ molecule^{-1}\ s^{-1}$; and termolecular, $cm^6\ molecule^{-2}\ s^{-1}$.
1. Measured [*Plane*, 2002]. 2. Estimated rate coefficient from electronic structure calculations on the relevant transition states (see text). 3. Measured [*Plane et al.*, 1990]. 4. Electronic structure calculations and RRKM theory (see text). 5. Electronic structure calculations and TST (see main text). 6. This reaction represents loss of $KHCO_3$ to meteoric smoke particles (see text). 7. Theory [*Plane et al.*, 2006]. 8. Estimate based on typical dissociative electron recombination reaction rates [*Florescu-Mitchell and Mitchell*, 2006]. 9. Electronic structure calculations using time-dependent density function theory (see text). 10. Estimate [*Swider*, 1970].

WACCM-K was run from 2004 to 2012 (after a 9 year spin-up), with dynamical fields nudged in the troposphere and stratosphere to the Goddard Earth Observing System-5 (GEOS-5) meteorological data set, as described by *Feng et al.* [2013]. A nudging coefficient value (0.01) was used when assimilating the GEOS-5 analysis into WACCM so that 1% of the meteorological conditions were combined with WACCM fields below 60 km at every model dynamics time step. Above 60 km the model was free running. The MIF is calculated from current knowledge of the astronomical characteristics of the sporadic meteor complex to estimate the

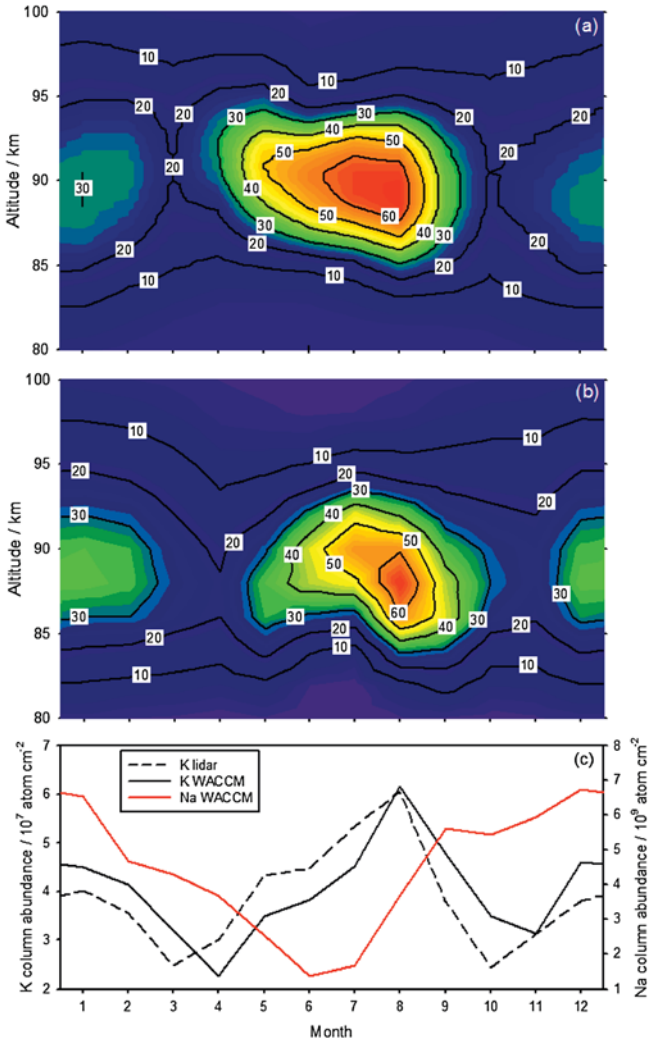

Figure 3. Annual variation of the K layer at Kühlungsborn, Germany (54°N, 12°E), averaged from 2004 to 2006. (a) K density (atom cm^{-3}) as a function of altitude and month, measured by lidar. (b) K density as a function of altitude and month from WACCM-K. (c) The observed and modeled K column abundance, compared with the Na column abundance (since Na lidar measurements are not available from Kühlungsborn for the same period, validated model output [*Marsh et al.*, 2013] for that location averaged over 2004–2006 is shown).

global meteoric mass flux deposited at each altitude within the MLT at all latitudes for each day of the year [*Fentzke and Janches*, 2008]. A chemical ablation model [*Vondrak et al.*, 2008] is then used to compute the injection rates of individual metallic elements as a function of altitude. See *Feng et al.* [2013] for further details.

The WACCM-K output was compared with lidar measurements of the K layer made over 3 years (2004–2006) at Kühlungsborn, Germany (54°N, 12°E) (see *Eska et al.* [1999] for a description of the technique). The K layer at this station is typical of other midlatitude locations [*Sullivan and Hunten*, 1964; *Megie et al.*, 1978]. To minimize the impact of solar cycle effects on the K layer, we focus here on the seasonal variation of the K layer averaged over the 3 years. Figure 3a shows the measured seasonal variation of the K density as a function of height, and Figure 3b shows the modeled variation. The first noteworthy point is that the semiannual variation of the K layer, with a midsummer maximum and minima at the equinoxes, is very well captured by the model. A second point is that the *absolute* K density agrees well with the observed density, using a MIF for K (average 120 atom $cm^{-2}\,s^{-1}$) which is in the chondritic ratio (K/Na = 6.5% [*Asplund et al.*, 2009]) to the Na MIF used in our recent study of the Na layer [*Marsh et al.*, 2013]. This is in accord with a chemical ablation model [*Vondrak et al.*, 2008] which predicts that Na and K should ablate with similarly high efficiencies compared to other meteoric metals. A third point is that the peak height and width of the layer are satisfactorily captured by the model (see Figure S2 in the supporting information which shows MLT profiles of all the K-containing species in WACCM-K). Figure 3c shows that the modeled semiannual seasonal variation of the K column abundance is also in good agreement with the lidar measurements. The contrasting seasonal variation of the Na layer at the same location [*Marsh et al.*, 2013] is included for comparison.

4. Discussion and Conclusions

Why does K exhibit a summertime peak and equinoctial minima, in contrast to Na? There are two factors involved. First, the K^+ ion is more difficult to neutralize because it can only form weakly bound cluster ions at very low temperatures. Thus, the low temperatures of the summertime MLT shift the balance from K^+ to K, accounting for the summertime maximum. The second factor concerns the neutral chemistry. None of the reactions involving KO, KO_2, and KOH has a significant temperature dependence. In contrast, the activation

energy for the reaction $KHCO_3 + H$ is so large that this reaction never plays a significant role, even during the warmest period in winter. The only route from $KHCO_3$ back to K is via photolysis, and this is essentially temperature independent. For Na, the reaction $NaHCO_3 + H$ has a smaller activation energy [*Cox et al.*, 2001], and so during winter this reaction becomes fast enough to recycle the reservoir to atomic Na, leading to the pronounced wintertime maximum. Because there is less winter-summer variation in the K layer, the semiannual variations become pronounced. As shown in Figure S3 (supporting information), atomic O exhibits minima at the equinoxes, whereas H_2 and CO_2 exhibit maxima. Inspection of Figure 1 shows that simultaneously decreasing O and increasing H_2 and CO_2 will drive K to $KHCO_3$, and this explains the minima in the K layer seen during the equinoxes.

It should be pointed out that the MIF used here would correspond to a global input rate of 4.6 t d^{-1} of ablated cosmic dust [*Marsh et al.*, 2013]. This is at the lower end of current estimates of this quantity, which vary from ~3 to 300 t d^{-1} [*Plane*, 2012]. Although this estimate is calculated from an astronomical model constrained to measurements of meteor head echoes using a number of high-performance large aperture radars [*Fentzke and Janches*, 2008], it is possible that a population of undetected meteors could make a significant contribution to the MIF. To test this possibility, we ran a sensitivity experiment where the MIF was increased by a factor of 10 in WACCM-K. The K column density increased by a factor of 8.6 (there is a small nonlinearity because of the second-order polymerization reaction R13 in Table 1). The coefficient of R13 would therefore need to be increased if the MIF was larger than 4.6 t d^{-1}. However, the layer height, the layer shape, and the semiannual seasonal behavior of the K layer—which is the focus of this study—were unchanged.

In conclusion, the surprisingly different behavior of the K layer now appears to be explained. Nevertheless, it would be desirable if the theoretical rate calculations presented here for reactions (13) and (14a)–(14c), and the assumed rate coefficients for reactions (8)–(12), could be tested experimentally in the future.

Acknowledgments

This work was supported by the UK Natural Environment Research Council (NERC grant NE/G019487/1) and the European Research Council (project 291332-CODITA). The data required for the rate coefficient calculations described in the paper are in Table S1 of the supporting information. Additional figures S1–S3, referred to in the text, are also included in the supporting information.

The Editor thanks two anonymous reviewers for their assistance in evaluating this paper.

References

Ager, J. W., and C. J. Howard (1987), Gas-phase kinetics of the reactions of NaO with H_2, D_2, H_2O, and D_2O, *J. Chem. Phys.*, *87*, 921–925.

Asplund, M., N. Grevesse, A. J. Sauval, and P. Scott (2009), The chemical composition of the Sun, *Annu. Rev. Astron. Astrophys.*, *47*, 481–522.

Bauernschmitt, R., and R. Ahlrichs (1996), Treatment of electronic excitations within the adiabatic approximation of time dependent density functional theory, *Chem. Phys. Lett.*, *256*, 454–464.

Cox, R. M., D. E. Self, and J. M. C. Plane (2001), A study of the reaction between $NaHCO_3$ and H: Apparent closure on the chemistry of mesospheric Na, *J. Geophys. Res.*, *106*(D2), 1733–1739, doi:10.1029/2000JD900579.

Delgado, R., B. R. Weiner, and J. S. Friedman (2006), Chemical model for mid-summer lidar observations of mesospheric potassium over the Arecibo Observatory, *Geophys. Res. Lett.*, *33*, L02801, doi:10.1029/2005GL024326.

Eska, V., U. von Zahn, and J. M. C. Plane (1999), The terrestrial potassium layer (75–110 km) between 71°S and 54°N: Observations and modeling, *J. Geophys. Res.*, *104*(A8), 17,173–17,186, doi:10.1029/1999JA900117.

Feng, W., D. R. Marsh, M. P. Chipperfield, D. Janches, J. Hoeffner, F. Yi, and J. M. C. Plane (2013), A global atmospheric model of meteoric iron, *J. Geophys. Res. Atmos.*, *118*, 9456–9474, doi:10.1002/jgrd.50708.

Fentzke, J. T., and D. Janches (2008), A semi-empirical model of the contribution from sporadic meteoroid sources on the meteor input function in the MLT observed at Arecibo, *J. Geophys. Res.*, *113*, A03304, doi:10.1029/2007JA012531.

Florescu-Mitchell, A. I., and J. B. A. Mitchell (2006), Dissociative recombination, *Phys. Rep.*, *430*(5–6), 277–374.

Frisch, M. J., et al. (2009), *Gaussian 09, Revision A.1*, Gaussian, Inc., Wallingford, Conn.

Georgievskii, Y., and S. J. Klippenstein (2005), Long-range transition state theory, *J. Chem. Phys.*, *122*, 194103.

Griffin, J., D. R. Worsnop, R. C. Brown, C. E. Kolb, and D. R. Herschbach (2001), Chemical kinetics of the NaO(A) + O(^{3}P) reaction, *J. Phys. Chem. A*, *105*(9), 1643–1648.

Helmer, M., and J. M. C. Plane (1993), A study of the reaction $NaO_2 + O$ -- > $NaO + O_2$—Implications for the chemistry of sodium in the upper atmosphere, *J. Geophys. Res.*, *98*(D12), 23,207–23,222, doi:10.1029/93JD02033.

Jegou, J. P., M. L. Chanin, G. Megie, and J. E. Blamont (1980), Lidar measurements of atmospheric lithium, *Geophys. Res. Lett.*, *7*(11), 995–998, doi:10.1029/GL007i011p00995.

Jegou, J. P., C. Granier, M. L. Chanin, and G. Megie (1985), General theory of the alkali metals present in the Earth's upper atmosphere. 2. Seasonal and meridional variations, *Ann. Geophys.*, *3*(3), 299–312.

Kopp, E. (1997), On the abundance of metal ions in the lower ionosphere, *J. Geophys. Res.*, *102*(A5), 9667–9674, doi:10.1029/97JA00384.

Langowski, M., C. V. Savigny, J. P. Burrows, W. Feng, J. M. C. Plane, D. R. Marsh, D. Janches, M. Sinnhuber, and A. C. Aikin (2014), Global investigation of the Mg atom and ion layers using SCIAMACHY/Envisat observations between 70 km and 150 km altitude and WACCM-Mg model results, *Atmos. Chem. Phys. Discuss.*, *14*, 1971–2019.

Lim, I. S., P. Schwerdtfeger, B. Metz, and H. Stoll (2005), All-electron and relativistic pseudopotential studies for the group 1 element polarizabilities from K to element 119, *J. Chem. Phys.*, *122*(10), 104103.

Marsh, D. R., D. Janches, W. Feng, and J. M. C. Plane (2013), A global model of meteoric sodium, *J. Geophys. Res. Atmos.*, *118*, 11,442–411,452.

Megie, G., F. Bos, J. E. Blamont, and M. L. Chanin (1978), Simultaneous nighttime lidar measurements of atmospheric sodium and potassium, *Planet. Space Sci.*, *26*(1), 27–35.

Montgomery, J. A., M. J. Frisch, J. W. Ochterski, and G. A. Petersson (1999), A complete basis set model chemistry. VI. Use of density functional geometries and frequencies, *J. Chem. Phys.*, *110*, 2822.

Plane, J. M. C. (2002), Laboratory studies of meteoric metal chemistry, in *Meteors in the Earth's Atmosphere*, edited by E. Murad and I. P. Williams, p. 309, Cambridge Univ. Press, Cambridge, U. K.

Plane, J. M. C. (2003), Atmospheric chemistry of meteoric metals, *Chem. Rev.*, *103*(12), 4963–4984.
Plane, J. M. C. (2004), A time-resolved model of the mesospheric Na layer: Constraints on the meteor input function, *Atmos. Chem. Phys.*, *4*, 627–638.
Plane, J. M. C. (2012), Cosmic dust in the Earth's atmosphere, *Chem. Soc. Rev.*, *41*, 6507–6518.
Plane, J. M. C., B. Rajasekhar, and L. Bartolotti (1990), Kinetic study of the reactions $K + O_2 + N_2$, $K + O_2 + He$ from 250 K to 1103 K, *J. Phys. Chem.*, *94*(10), 4161–4167.
Plane, J. M. C., R. J. Plowright, and T. G. Wright (2006), A theoretical study of the ion-molecule chemistry of $K^+.X$ complexes (X = O, O_2, N_2, CO_2, H_2O): Implications for the upper atmosphere, *J. Phys. Chem. A*, *110*(9), 3093–3100.
Robertson, S. H., D. R. Glowacki, C.-H. Liang, C. Morley, R. Shannon, M. Blitz, and M. J. Pilling (2008), MESMER (Master Equation Solver for Multi-Energy Well Reactions), 2008–2012: An object oriented C^{++} program for carrying out ME calculations and eigenvalue-eigenvector analysis on arbitrary multiple well systems, edited. [Available at http://sourceforge.net/projects/mesmer.]
Self, D. E., and J. M. C. Plane (2002), Absolute photolysis cross-sections for $NaHCO_3$, NaOH, NaO, NaO_2 and NaO_3: Implications for sodium chemistry in the upper mesosphere, *Phys. Chem. Chem. Phys.*, *4*(1), 16–23.
Sullivan, H. M., and D. M. Hunten (1964), Lithium, sodium and potassium in twilight airglow, *Can. J. Phys.*, *42*(5), 937–956.
Swider, W. (1970), Ionic reactions for meteoric elements, *Ann. Geophys.*, *26*(2), 595–600.
Vondrak, T., J. M. C. Plane, S. Broadley, and D. Janches (2008), A chemical model of meteoric ablation, *Atmos. Chem. Phys.*, *8*(23), 7015–7031.